Received: 18 February 2021 | Revised: 26 June 2021

DOI: 10.1111/sapm.12433

SPECIAL ISSUE

STUDIES IN APPLIED MATHEMATICS WILEY

Molecular dynamics simulations to explore the structure and rheological properties of normal and hyperconcentrated airway mucus

Andrew G. Ford[1] | **Xue-Zheng Cao**[2] | **Micah J. Papanikolas**[3] | **Takafumi Kato**[4] | **Richard C. Boucher**[4] | **Matthew R. Markovetz**[4] | **David B. Hill**[4,5] | **Ronit Freeman**[3] | **Mark Gregory Forest**[1,3,6]

[1] Department of Mathematics, University of North Carolina at Chapel Hill, Chapel Hill, North Carolina, USA

[2] Department of Physics, Xiamen University, Xiamen, China

[3] Department of Applied Physical Sciences, University of North Carolina at Chapel Hill, Chapel Hill, North Carolina, USA

[4] Marsico Lung Institute, University of North Carolina at Chapel Hill, Chapel Hill, North Carolina, USA

[5] Department of Physics and Astronomy, University of North Carolina at Chapel Hill, Chapel Hill, North Carolina, USA

[6] Department of Biomedical Engineering, University of North Carolina at Chapel Hill, Chapel Hill, North Carolina, USA

Correspondence
Mark Gregory Forest and Andrew G. Ford, Department of Mathematics, University of North Carolina at Chapel Hill, 329 Phillips Hall, Chapel Hill, NC 27599.
Email: forest@unc.edu and agford@live.unc.edu

Funding information
Cystic Fibrosis Foundation; National Science Foundation; National Center for Advancing Translational Sciences; National Institutes of Health

Abstract

We develop the first molecular dynamics model of airway mucus based on the detailed physical properties and chemical structure of the predominant gel-forming mucin MUC5B. Our airway mucus model leverages the LAMMPS open-source code [https://lammps.sandia.gov], based on the statistical physics of polymers, from single molecules to networks. On top of the LAMMPS platform, the chemical structure of MUC5B is used to superimpose proximity-based, noncovalent, transient interactions within and between the specific domains of MUC5B polymers. We explore feasible ranges of hydrophobic and electrostatic interaction strengths between MUC5B domains with 9 nm spatial and 1 ns temporal resolution. Our goal here is to propose and test a mechanistic hypothesis for a striking clinical observation with respect to airway mucus: a 10-fold increase in nonswellable, dense structures called flakes during progression of cystic fibrosis disease. Among the myriad possible effects that might promote self-organization of MUC5B networks into flake structures, we hypothesize and confirm that the clinically confirmed increase in mucin concentration, from 1.5

to 5 mg/ml, alone is sufficient to drive the structure changes observed with scanning electron microscopy images from experimental samples. We postprocess the LAMMPS simulated data sets at 1.5 and 5 mg/ml, both to image the structure transition and compare with scanning electron micrographs and to show that the 3.33-fold increase in concentration induces closer proximity of interacting electrostatic and hydrophobic domains, thereby amplifying the proximity-based strength of the interactions.

KEYWORDS
molecular dynamics, mucus, rheology

1 | INTRODUCTION

Mucus is a complex mixture of proteins, salts, lipids, and water that forms a hydrogel within the lumen of many organs, including the respiratory, gastrointestinal, and reproductive systems.[1–7] The primary components of mucus are high molecular weight polymers called mucins. Airway mucus is composed of two mucins, MUC5B (most predominant) and MUC5AC.[8–10] The mucus layer within the lung provides a total air-mucus surface area approximately the size of a tennis court. This interface allows the mucus to cleanse inhaled air of trapped particulates, cellular fragments, pathogens, and dead cells.[7,11] Coordinated cilia propel the mucus barrier toward the trachea, creating an escalator-like transport of the mucus layer to be swallowed along with trapped cargo into the acidic environment of the stomach; this mechanism is known as mucociliary clearance. As a result, the airway mucus barrier is continuously replenished by production of MUC5B primarily by submucosal glands and MUC5AC primarily by goblet cells.[12]

In muco-obstructive diseases, such as chronic obstructive pulmonary disease (COPD) and cystic fibrosis (CF), mucus becomes dehydrated,[8,13–15] leading to elevated and eventually hyperelevated mucin concentrations. The resulting mucus possesses aberrant viscous and elastic properties that obstruct mucociliary clearance, with significant health consequences. In healthy humans, airway mucin concentrations are approximately 1–2 mg/ml; during CF, mucin concentrations elevate to 5–10 mg/ml in advanced stages.[8,14] In addition to hyperconcentration, as CF progresses, the mucins self-assemble to form high-density nonswellable structures called flakes.[16] The formation of flakes in animals with bronchitis and their role in compromised mucociliary transport of mucus was recognized a half-century ago.[17] Flakes account for approximately 5% of the mucins in healthy airway mucus samples, progressing to approximately 50% of the mucins in airway mucus of advanced CF samples.[16] The underlying physical and chemical mechanisms that promote and sustain flake formation remain unknown, the motivation for this study.

In this paper, we use physics- and chemistry-based computational modeling tools to explore the interplay between MUC5B concentration and noncovalent, transient, electrostatic, and hydrophobic interactions within and between domains of MUC5B polymers that: (i) promote structure transitions in the mucin network; and (ii) facilitate flake formation. Our approach is guided by exper-

imental scanning electron microscopy (SEM) images of the network structure of mucus at two different mucin concentrations, one (1.5 mg/ml) consistent with healthy samples and another (5 mg/ml) with hyperconcentrated CF mucus samples. As detailed below, there has been no evidence to date that the transitions observed from healthy to diseased CF states of airway mucus are associated with aberrant structure changes in individual airway mucin molecules, MUC5B or MUC5AC, as established decades ago with the primary mucin molecule MUC2 in gastric mucus (see next paragraph). Rather, in airway mucus, a myriad of conditions alter the transient interactions between domains within the fundamental MUC5B, MUC5AC monomers, the fundamental units that comprise mucin polymers. The focus of this paper is to use molecular dynamics (MD) simulations, image processing, and proximity statistics of interacting domains from simulated data, guided by experimental electron microscopy images, to test and confirm our hypothesis that flake-like structure transitions in the MUC5B network are possible purely by virtue of elevated mucin concentration from 1.5 to 5 mg/ml. This result is only one step toward impacting clinical treatment. Nonetheless, it does suggest a focus on hydration of the airways to combat structure transitions in disease progression, and only if that fails, to explore additional potential causes. In addition, this modeling platform provides a platform to test subsequent strategies such as mucolytic drugs that target the transient electrostatic and hydrophobic interaction domains.

Research on the intricate mechanisms that regulate mucus rheology has progressed along several directions, dating back to the 1950s[18] and subsequently in the 1990s[19,20] as the genomic basis of mucins was being revealed. In gastrointestinal mucus, the groups of Bansil and Urbanc,[21–28] together with medical colleagues, made significant advances in understanding the critical role of pH in protecting the epithelium of the stomach and intestinal tract, combining various imaging microscopy and bulk rheological techniques with discrete MD simulations. Their simulations focused on normal and anomalous protein folding of the gel-forming gastric mucin MUC2, revealing a highly local structure transition; individual beads in the bead-spring polymer model were discretized to match the size of amino acids, using the GROMACS software package.[29,30] These studies revealed a pH-dependent structure transition at the scale of individual proteins,[21,24,28] leading at successively larger scales to mucin aggregation at low pH; furthermore, in Refs. 25, 26, the connection was established between pH-dependent protein conformation changes confirmed by electron microscopy and MD simulations and a macrorheological (i.e., bulk) sol–gel transition measured at the bulk scale with rheometers. Animal clinical trials have been especially valuable in providing sufficient volumes of gastrointestinal mucus to perform standard macrorheological experiments (e.g., with cone and plate rheometers), providing a key link between structure at the single molecule and molecular network scales and bulk rheology. These mechanistic insights guided subsequent drug treatments to restore normal gastric pH levels.

In CF, several investigators[31] have pursued the natural hypothesis that pH is the underlying cause of abnormal airway mucus. However, CF is a genetic disease, arising from the defective function of the cystic fibrosis transmembrane conductance regular (CFTR); this defective ion channel obstructs normal hydration of the airway surface, leading to mucus hyperconcentration.[12] Furthermore, the protective barrier function of gastric mucus is precisely to manage the dramatic pH-gradient between the epithelium and the internal acidic contents. The airway mucus barrier serves a dramatically different function, to trap inhaled insults (particulates and pathogens) and transport them to be swallowed into the acidic gastrointestinal tract. Several studies[14,16,32,33] have provided compelling evidence that the disease progression of airway mucus in CF results from increasingly higher concentrations of mucins (MUC5B primarily), and not from low pH. Thus, the cascade in mucus structure and rheology during CF progression is not known to induce anomalous MUC5B or MUC5AC folding at the amino acid scale. Alternatively, we surmise that

the CF cascade arises as the proximity of MUC5B domains in more concentrated states amplifies the effects of the transient hydrophobic and electrostatic interactions between domains within MUC5B monomers, leading to a network structure transition. We test this hypothesis in this paper, and indeed confirm a rise in concentration of MUC5B from 1.5 to 5 mg/ml is sufficient to induce a structure transition by shifting the proximity distribution of electrostatic and hydrophobic domains within and between MUC5B polymers and thereby amplifying the transient interactions.

We take the opportunity here to highlight significant hurdles that continue to obstruct experimentally informed computational modeling and simulations of respiratory tract mucus, both for the flow transport of mucus in the airways or cell cultures (cf. Refs. 34–36) as well as the diffusive transport of different sizes and chemical properties of foreign species (small molecule drugs, drug carrier particles, pathogens, particulates, and passive tracers) embedded within mucus (cf. Refs. 30, 31, 37–40). Decades of development of hydrodynamic modeling and numerical methods for polymeric fluids (cf. Refs. 41, 42) have focused on generalizing the Navier–Stokes equations for the incompressible velocity field to include new degrees of freedom arising from the polymer network. The divergence of stress terms in the momentum balance include the standard viscous stress tensor (symmetrized velocity gradient), plus one additional "extra stress contribution" for each polymer-induced relaxation mode. To close the system, a corresponding Maxwell-like hyperbolic transport equation is given for each extra stress mode. We refer to Ref. 36 for a five-mode extra stress model of mucus transport in cell cultures, where the extra stress modes are fitted to approximate macrorheology data. The limitation of this approach is that the *linear* rheology of pulmonary mucus reveals a power-law behavior of the time-dependent viscous and elastic moduli, whereas Maxwell extra stress models are an exponential basis. In Ref. 36, we show that even for linear responses of bronchial mucus, five modes are not sufficient to quantitatively fit the power law. Even worse, there are no known ways to parameterize and fit the nonlinear response modes of mucus to large amplitude stress and strain data. And further, there are no known constitutive laws and numerical methods for the nonlinear response of power-law complex fluids. As a result, rheologically faithful hydrodynamic simulations of airway mucus remain wide open.

These limitations have inspired the approach taken in the present paper to focus on the mucus structure that underlies flow transport. To do this, we develop an MD model of the linear viscoelastic behavior of pulmonary mucus, anchored in the detailed chemistry of mucins, MUC5B in particular, and the transient interactions within and between different domains of MUC5B monomers and dimers. This modeling approach has the ability to synthetically reproduce the linear, equilibrium structure of the network over ranges of transient interaction strengths and MUC5B concentrations, which we then compare against structure images from electron microscopy. The MD simulations further predict, by postprocessing of the simulated data from statistical physics summation formulas, the equilibrium linear viscoelastic moduli at the frequencies resolved by the simulations. These results are analogous to MD simulations of pig gastric mucus by Bansil and Urbanc,[21,24,28] but we focus on the network structure as opposed to single protein folding structure at the fine scales of amino acid resolution due to pH of the solvent. To our knowledge, results presented in this paper are the first MD simulations of human pulmonary mucus network structure based on the physicochemical properties of the primary, gel-forming mucin, MUC5B.

MD models of polymer networks begin by discretizing segments of each polymer chain into beads connected by nonlinear (finitely extensible) springs, where nonneighboring beads within or between chains interact with each other through the use of potential functions that reflect the mucin polymer chemistry at monomeric and dimeric scales. In the 1990s, Kremer and Grest[43] published an MD model utilizing the Lennard-Jones "12-6" potential, and analogs of this MD platform

have been widely used ever since, with Grest leading the open source LAMMPS software development at Sandia National Laboratory. Here, we adapt this software platform to represent and study the rheology of MUC5B-dominated lung mucus, exploring one healthy and one relatively high mucin concentration, and for each a range of transient interaction strengths between MUC5B domains. Our model and simulations operate at smaller length scales and shorter timescales than standard rheological laboratory techniques, providing an extension of existing rheological data, while directly comparable experimental evidence is provided by electron microscopy images that we synthetically generate by imaging the simulated data and then compare.

Section 2.1 outlines the setup of model, covering the representation of mucus and the derivation of the physical unit scales used in the model. In addition, this section gives details on the potentials that govern transient bead–bead interactions within the model. Section 2.2 covers the data analysis techniques used to derive the viscoelastic properties of mucus from the model output. Section 2.3 describes the laboratory imaging technique used as a basis to verify structures produced in the model. Section 3 gives an analysis of model-generated images and the computed rheological moduli from Section 2.3, establishing a link between the spectrum of moduli and structures. This link can help predict the underlying mucus structures at various parameter ranges, a useful tool in the future study of medications to manage muco-obstructive diseases.

2 | METHODS

2.1 | Physicochemical polymer representation of MUC5B mucins

Our model is implemented using the software package LAMMPS,[44] published by Sandia National Labs [http://lammps.sandia.gov]. In physiology, mucins are organized as polymers, where each monomer spans approximately 500 nm (Figure 1a).[45] We focus on the structure of MUC5B in the model as it is the predominant gel-forming mucin found within airway mucus. At each protein terminus, there are large cysteine containing domains that allow mucins to form polymers that are linked N–N and C–C through covalent disulfide bonds. In between the termini, the protein consists of a mixture of glycosylated domains and cysteine knots. Mucin domains contain multiple random repeats of three amino acids: proline, threonine, and serine. These residues form a central backbone that is highly glycosylated through alcohol groups on threonine and serine residues. This sugar brush comprises over 50% of the mucin molecular weight.[45] These glycosylations have been shown to change within CF disease states.[46,47]

To simulate mucus gels across concentration and transient affinities between nonneighboring beads, we have to introduce some coarse-graining. We choose a resolution where one mucin monomer is composed of 57 beads in a linear chain (Figure 1b). These monomers were linked together to form dimers, and each polymer chain consists of five dimers. The diameter of each bead is set to 9 nm. This size is chosen for two reasons: first, it approximates the diameter of the portion of the mucin polymer with polysaccharide side chains, and second, it approximates the persistence length of a MUC5B mucin chain.[48,49]

We then divided the mucin beads into three blocks containing either (1) portions of the termini, (2) cysteine knots, or (3) electrostatic interactions. Beads associated with the protein termini and the cysteine knots were assigned the same hydrophobic interactions, due to the inherent hydrophobicity of the peptide backbone; however, cysteine knots are often spatially shielded from other beads due to their locations between the mucin domains. The beads located within the mucin domains are heavily decorated with a glycan brush.[37] These regions can experience a

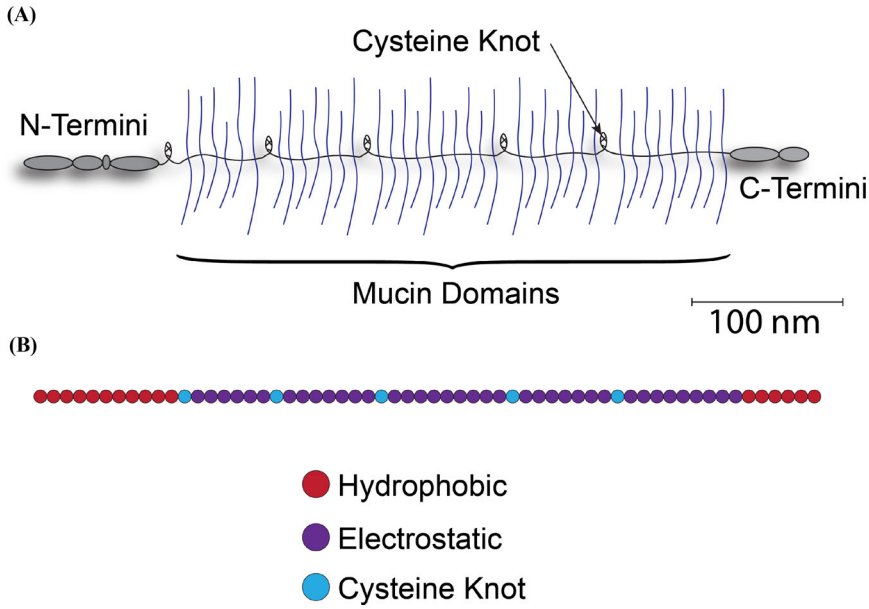

FIGURE 1 The representation of one mucin monomer in the model. Termini (red) experience hydrophobic interactions, while sugar domains (purple) and cysteine knots experience electrostatic interactions

variety of interactions such as hydrogen bonding or ionic bonds. The saltwater solvent of mucus is represented implicitly through an overdamped Langevin thermostat.[50,51] In addition, as ions found within the solvent facilitate electrostatic interactions between mucin polymers, the effects of the ions in the solvent on transient electrostatic interactions are also implicitly represented through the usage of potential functions. In this study, we focus on MUC5B chain networks at two different concentrations, and explore the strengths of interactions within and between the mucin chains. These interaction strengths are a product of many other diverse molecular species that are present in airway mucus and that can either suppress or enhance mucin–mucin interactions, for example, through binding of those molecular species to mucin domains as explored in Ref. 52.

The simulation itself is nondimensionalized based on choices made for the units for length and mass.[53] In this model, the length unit σ is set to 9 nm to match the diameter of the bead. The mass unit m is set to the mass of one bead; we assume that all beads have equal mass because the overdamping of the Langevin thermostat removes inertia from the simulation. The energy unit ε_0 is set to $k_B T$, where T represents the temperature in Kelvin. Experimental simulations are run at $37℃ = 310$ K to match human body temperature, so we use this value for T in our simulations. For thermodynamic consistency, the energy unit must satisfy the relation $\varepsilon_0 = \frac{m\sigma^2}{\tau_0^2}$, which requires the simulation time step τ_0 to be on the order of 1 ns. This internal consistency has important consequences with respect to the timescales we are able to simulate, and therefore the frequency range in transform space.

From estimates of the concentration of mucins within mucus,[8,14] we represent two different concentrations of mucins in our model: 1.5 mg/ml mucins to represent a healthy person, and 5.0 mg/ml mucins to represent the low end of the CF concentration range. We underscore that the volume fractions taken up by the polymer chains are higher than the mucin concentrations would

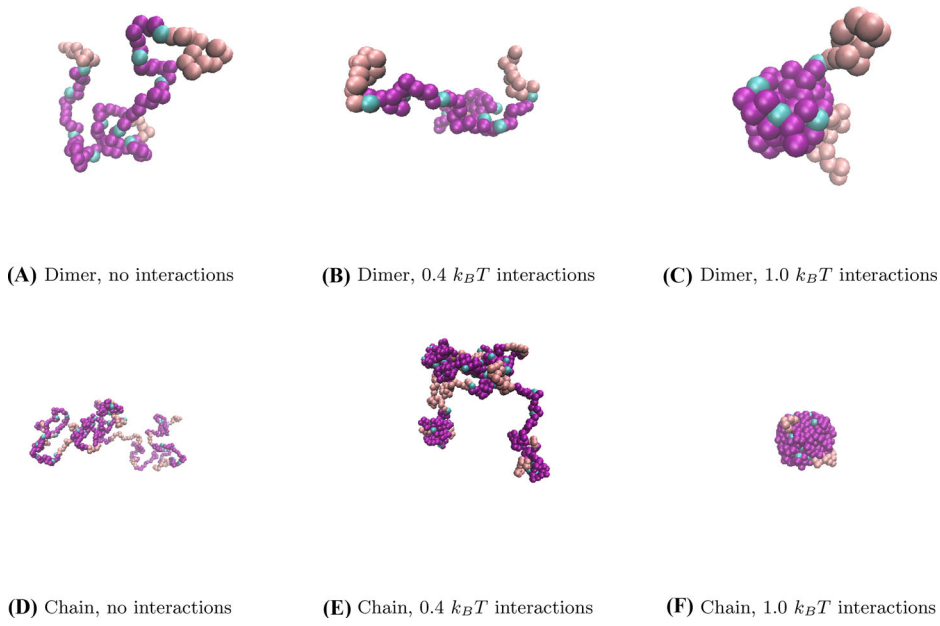

(A) Dimer, no interactions **(B)** Dimer, 0.4 k_BT interactions **(C)** Dimer, 1.0 k_BT interactions

(D) Chain, no interactions **(E)** Chain, 0.4 k_BT interactions **(F)** Chain, 1.0 k_BT interactions

FIGURE 2 Images taken from simulations of a single dimer (a–c) and single chain (d–f) at various interaction strengths

suggest, as the spherical bead shapes used in the model encompass some volume taken up by the solvent in the experimental setting and are therefore larger than the mucins they represent. The 1.5 mg/ml mucus model has a volume fraction of approximately 3.2% taken up by the beads, while the 5.0 mg/ml mucus model has a volume fraction of approximately 10.7%.

To test our simulation methods, we simulated a single MUC5B dimer and a single MUC5B 5-dimer polymer using our model with a feasible range of interaction strengths, in addition to simulations where transient interactions are eliminated entirely (Figure 2)[54]; the latter simulations are used to benchmark the baseline model through comparisons to known theory on Rouse chains.[55,56] The data in Figure 3 indicate that the baseline polymer melt is sol-like for most frequencies in the range measure, but gel-like at the upper edge of the frequency range.

The model is implemented with periodic boundary conditions, allowing beads to freely pass through and interact across boundaries. The box size is 900 nm, or 100 times the diameter of a bead. As mucins are represented as polymers with $N = 570$ beads each, the average radius of gyration of a single chain experiencing no attractive interactions is given in Equation (1)[56]

$$\langle R_g \rangle = \sqrt{\frac{N\sigma^2}{6}} \approx 9.75\sigma \approx 87.7\,\text{nm}. \tag{1}$$

However, the presence of attractive interactions, especially when gels form involving several polymer chains, complicates calculations of the radius of gyration for the full system. Therefore, we choose a box size much larger than the radius of gyration to mitigate complicating factors.

The structure of the model and its potential functions are derived from the classical Kremer–Grest polymer model.[43,55] This model represents polymers as chains of beads; beads are bonded to their neighbors by nonlinear, finitely extensible, spring potentials. Beads also experience excluded-volume interactions with other beads. Our model adds attractive forces to represent spe-

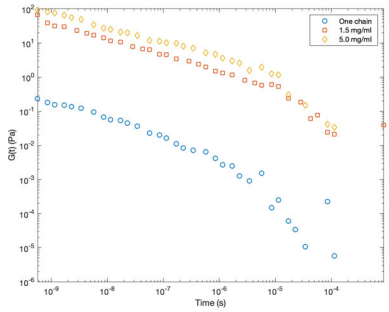

(A) $G(t)$

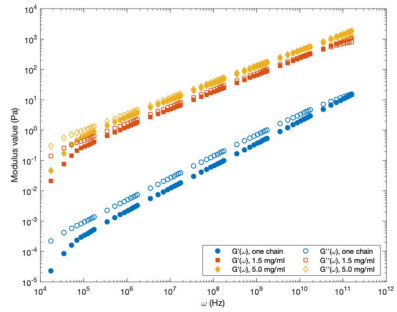

(B) $G'(\omega)$ and $G''(\omega)$

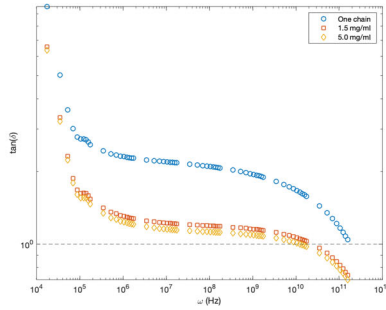

(C) $\tan(\delta)$; horizontal line represents $\tan(\delta) = 1$.

FIGURE 3 Rheological data from simulations of a single chain, 1.5 mg/ml mucin simulation, and 5.0 mg/ml mucin simulation, respectively. All chains have bead number $N = 570$

cific chemical interactions between certain domains (beads) of the polymers, and the strengths of those interactions are what we aim to infer based on comparisons of the structures of simulations and microscopy images.

Interactions between nonbonded beads separated by a distance r are represented by the Lennard-Jones "12-6" potential function:

$$U = 4\varepsilon\left[\left(\frac{\sigma}{r}\right)^{12} - \left(\frac{\sigma}{r}\right)^{6}\right] + C, \quad r < r_c. \tag{2}$$

The parameter σ represents the diameter of the beads; in our model, this matches the base length unit and is set to 1. The value of C is chosen for computational reasons to ensure continuity of the potential function; it is chosen to ensure $U = 0$ at the cutoff radius $r = r_c$. For interactions between nonbonded and nonattracted beads, the value of ε is set to 1.0 k_BT and $r_c = 2^{1/6} \cdot \sigma$; for attractive interactions, the value of ε is set to the interaction strength and $r_c = 2.5\sigma$. This cutoff is implemented for computational speed, as the potential function is very close to its $r \to \infty$ limit of 0 at this distance.

The minimum depth of the potential well in the Lennard-Jones potential occurs at $2^{1/6}\sigma$, the value which is also used as the cutoff radius for pairs of beads not experiencing attractive interactions. The attractive interactions reach their peak strength at the distance of $r = \sqrt[6]{\frac{26}{7}}\sigma$, where $\frac{dU}{dr}$ is maximized; the nondimenzionalized value of this force is more than double the value of ϵ/τ.

The original finitely extensible nonlinear elastic (FENE) bond in the Kremer–Grest model[43] is used here:

$$U = -0.5KR_0^2 \ln\left[1 - \left(\frac{r}{R_0}\right)^2\right] + 4\varepsilon\left[\left(\frac{\sigma}{r}\right)^{12} - \left(\frac{\sigma}{r}\right)^{6}\right] + \varepsilon. \tag{3}$$

In this function, the parameters are set as $K = 30.0$, $R_0 = 1.5\sigma$, $\varepsilon = 1.0$, and $\sigma = 1.0$. Here, as in the Lennard-Jones potential, ε and σ are the nondimensionalized energy and length units from the simulation, where $\varepsilon = k_BT$ and σ is the bead diameter.

2.2 | Data analysis

The global pressure tensor, an average of the per-bead stress tensor[57] scaled by the volume of the simulation domain, is used to estimate the stress relaxation modulus $G(t)$ by taking the ensemble average of the stress tensor σ at various lag times.[58] Here, $P^{\alpha\beta}$ represents the $\alpha\beta$ component of the pressure tensor, where α and β can represent x, y, or z. For a discrete selection of lag times t, the correlation function is taken for the xy-, xz-, and yz-components of the pressure tensor, and these values are ensemble averaged over nonoverlapping time windows to give the value of $G(t)$ at these lag times.

$$G(t) = \langle P^{\alpha\beta}(\tau)P^{\alpha\beta}(t+\tau)\rangle_{\alpha\neq\beta\in\{x,y,z\}}. \tag{4}$$

Using these data (Figure 8), a power-law fit is computed and used to generate the storage modulus G', which measures stored elastic energy, and loss modulus G'', which measures energy dissipation, across a range of frequencies using the following Fourier transform method specific to polymer gels[56]:

$$G'(\omega) = G_{eq} + \omega\int_0^\infty \left[G(t) - G_{eq}\right]\sin(\omega t)\,dt, \tag{5}$$

$$G''(\omega) = \omega\int_0^\infty \left[G(t) - G_{eq}\right]\cos(\omega t)\,dt, \tag{6}$$

$$\tan(\delta) = \frac{G''(\omega)}{G'(\omega)}, \tag{7}$$

where G_{eq} is defined as

$$G_{eq} = \lim_{t\to\infty} G(t). \tag{8}$$

In polymer melts and solutions, the value of δ found through the computation of $\tan(\delta)$ indicates the phase angle between the stress and applied strain within the system. In addition, where G' is larger than G'', the polymer network is gel-like (elasticity dominates viscosity at those fre-

quencies), whereas, $G'' > G'$ corresponds to sol-like behavior where viscosity dominates elasticity. We anticipate gel-like properties will dominate flake structures while sol-like properties will prevail in normal mucus or outside flakes in unhealthy mucus.

Given the timescale of our simulation, this model allows for the computation of G' and G'' at frequencies which are inaccessible via other rheological computation methods such as particle tracking.

2.3 | Scanning electron microscopy

Scanning Electron Microscopy on Human Bronchial Epithelial (HBE) mucus. Mucus samples were coated onto an APTES coated coverslip, and cross-linked with a solution containing 2.5% Gluteraldehyde, 2.0% Paraformaldehyde (PFA) in phosphate buffered saline (PBS) for 15 min. To preserve the microstructure of the mucins, the sample was then dehydrated with ethanol and critical point dried. The sample was imaged on a FEI Helios 600 Nanolab at 5 kV accelerating voltage (Figure 4).

3 | RESULTS AND DISCUSSION

Through the position data output from simulations, images, and videos were created using the imaging software VMD.[54] The images and videos indicated that all simulations reached a "quasi-equilibrium," where the visual state of the simulation stayed visually consistent except for very minor changes due to stochastic noise. Within these simulation videos, visible structures formed at interaction strengths of 0.6 k_BT and greater in the model with a mucin concentration of 1.5 mg/ml (Figure 5d–F). No visible structures formed at lower interaction strengths (Figure 5b,c) or in the baseline model with no attractive interactions (Figure 5a). Simulations were run for much longer than was needed to produce a visible "quasi-equilibrium" state, where a mostly stable structure varies only by minor stochastic noise.

As interaction strengths increase further at 1.5 mg/ml concentration, a very slow transition occurs in the network, with first signs of a few thin and one large strand coming out of the entangled MUC5B bundles shown at all lower interaction strengths. A network permeated by strands, similar to the SEM images of flakes in Figure 4, only forms at 1.5 mg/ml with the unrealistically high interaction strength of 4.0 k_BT; this high interaction strength creates long-lived transient bonds between interacting domains. Given the difference in scale between the simulation images (Figures 5 and 6), the simulated images with interaction strengths of 0.7 k_BT match the networks found in Figure 4c–d. Note that a single chain with weaker (1.0 k_BT) interactions collapses into a dense ball, whereas a 1.5 mg/ml concentration of chains starts to emit a few strands at 0.7 k_BT, but an unrealistically high interaction strength is needed to drive formation of a network of dense domains connected by thin strands as seen in flakes (Figure 4a). In simulations with these extremely strong attractive forces, individual beads quickly form a rigid network and transient bonds last sufficiently long to prevent further collapses into thicker strands or into the bundles at lower strengths.

At 5.0 mg/ml, MUC5B networks undergo a transition from uniform entangled bundles to formation of strands and a network of connected strands at much lower, and physically feasible, interaction strengths; the structure with 1.0 k_BT interactions is similar to the flake structure morphology seen in Figure 4. We therefore find that flake-like morphologies self-assemble in MUC5B net-

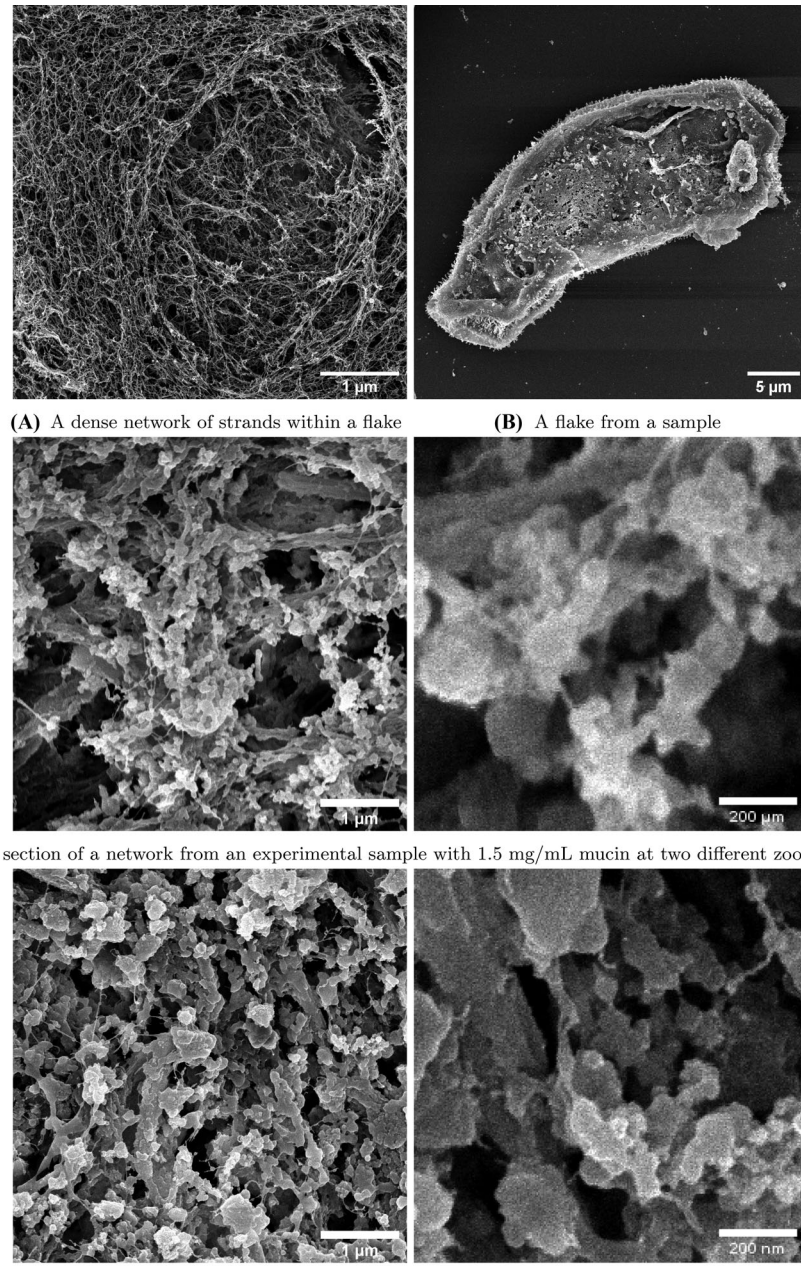

(A) A dense network of strands within a flake

(B) A flake from a sample

(C) A section of a network from an experimental sample with 1.5 mg/mL mucin at two different zoom levels

(D) A section of a network from an experimental sample with 5.0 mg/mL mucin at two different zoom levels

FIGURE 4 SEM images of various experimental mucus samples

works at the pathological CF concentration of 5.0 mg/ml with electrostatic and hydrophobic interaction potentials between domains at realistic strength of 1.0 k_BT. To the contrary, these strand-permeated flake morphologies do not form at the healthy concentration of 1.0 mg/ml at the same interaction potential strengths, requiring unrealistic potentials to do so. These results point to a deeper study of the simulation data sets to quantify the natural hypothesis that a 3.33-fold increase in concentration of MUC5B mucins, from 1.5 to 5.0 mg/ml, leads to closer proximity of domains on

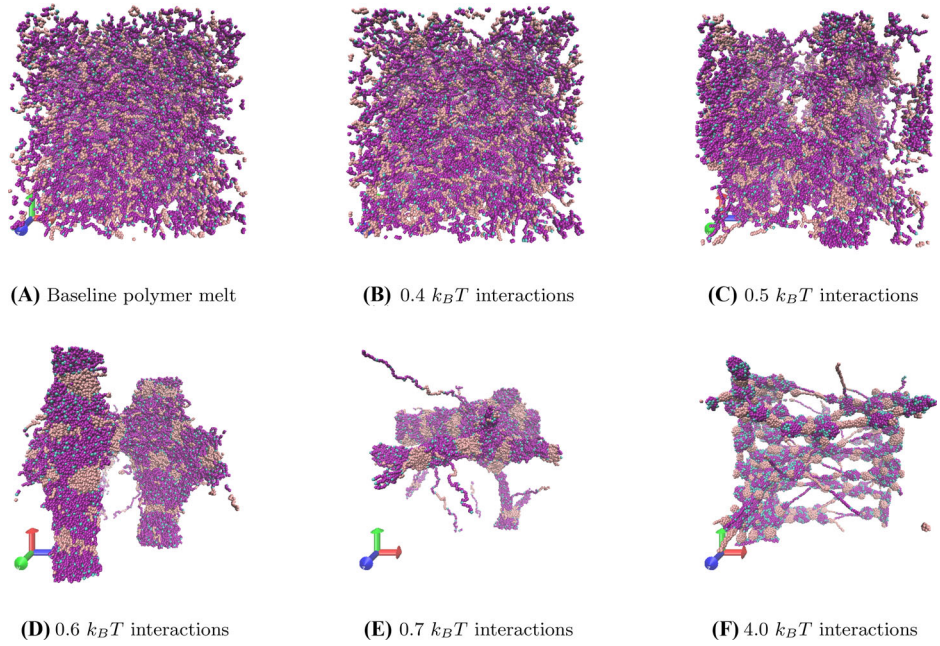

(A) Baseline polymer melt **(B)** 0.4 k_BT interactions **(C)** 0.5 k_BT interactions

(D) 0.6 k_BT interactions **(E)** 0.7 k_BT interactions **(F)** 4.0 k_BT interactions

FIGURE 5 A selection of images generated from simulations at various interaction strengths of HBE mucus with mucin concentration 1.5 mg/ml. All simulations reached quasi-equilibrium states, which are depicted in these images

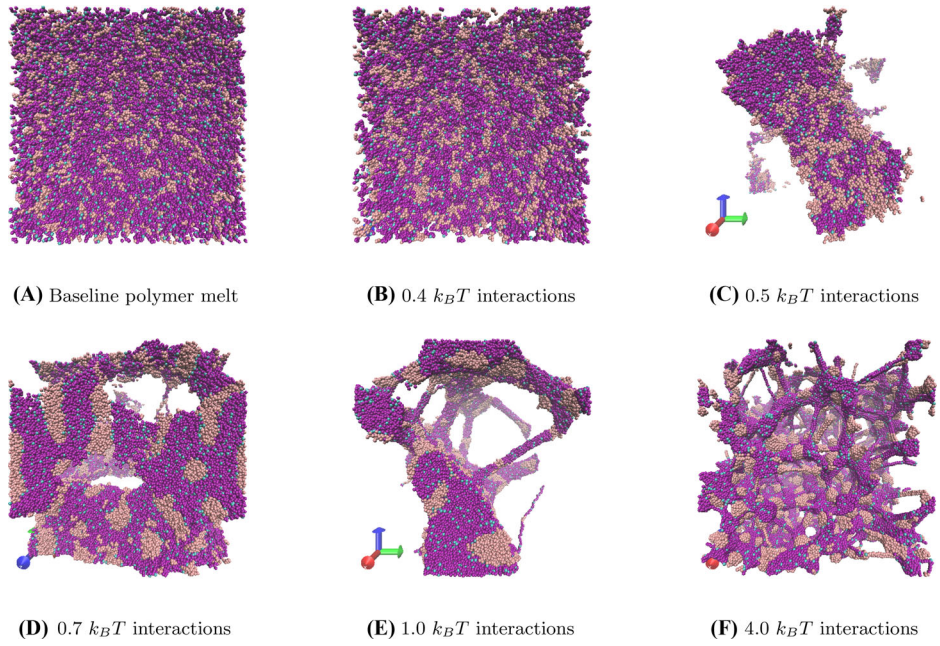

(A) Baseline polymer melt **(B)** 0.4 k_BT interactions **(C)** 0.5 k_BT interactions

(D) 0.7 k_BT interactions **(E)** 1.0 k_BT interactions **(F)** 4.0 k_BT interactions

FIGURE 6 A selection of images generated from simulations at various interaction strengths of HBE mucus with mucin concentration 5.0 mg/ml. All simulations reached quasi-equilibrium states, which are depicted in these images

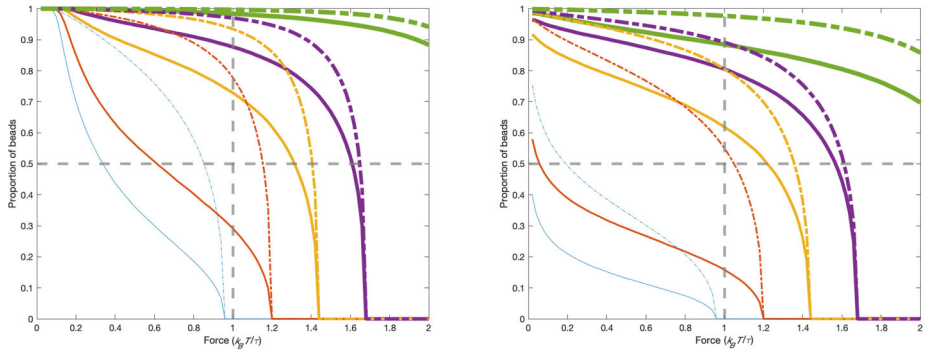

(A) All pairs of nonbonded beads **(B)** All pairs of beads on separate chains

FIGURE 7 The proportion of beads in all nonbaseline simulations which experience attractive interactions of various strengths. Solid lines represent simulations with mucin concentration 1.5 mg/ml, and dashed lines represent simulations with mucin concentration 5.0 mg/ml. Gray lines represent a force of 1.0 $k_B T/\tau$ and a proportion of 0.5. Blue lines represent 0.4 $k_B T$, orange represents 0.5 $k_B T$, yellow represents 0.6 $k_B T$, purple represents 0.7 $k_B T$, and green represents 1.0 $k_B T$

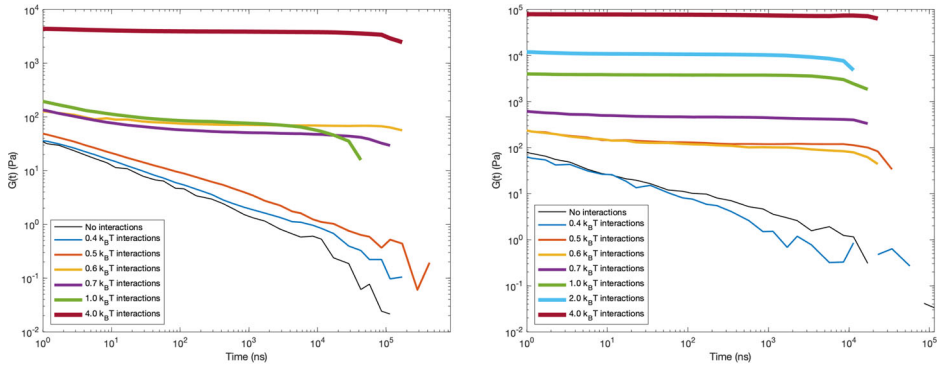

(A) Mucin concentration 1.5 mg/mL **(B)** Mucin concentration 5.0 mg/mL.

FIGURE 8 Plots of the stress relaxation function at the interaction strengths tested. Thicker lines correspond to stronger interactions

MUC5B that experience electrostatic and hydrophobic interactions, and because these potentials are proximity-based, the increase in concentration amplifies the strengths of those interactions.

To quantify the formation of permanent structures, we study the proportion of beads experiencing an attractive force stronger than 1.0 $k_B T/\tau$; this value represents the average strength of the random noise from the beads' interaction with the implicit solvent. In the simulations where well-defined structures appear to form, the majority of beads experience an attractive interaction of 1.0 $k_B T/\tau$ or stronger with at least one other bead (Figure 7). Attractive interactions of this strength are only possible when beads are located in close proximity to each other, indicating that this result stems from the increased concentration of the polymer chains within the simulated mucus. This suggests that the structures are generally permanent enough to withstand the stochastic noise in the simulation and quantifies the difference between well-defined structures and simulations without structures. In addition, this trend holds when limiting the same analysis

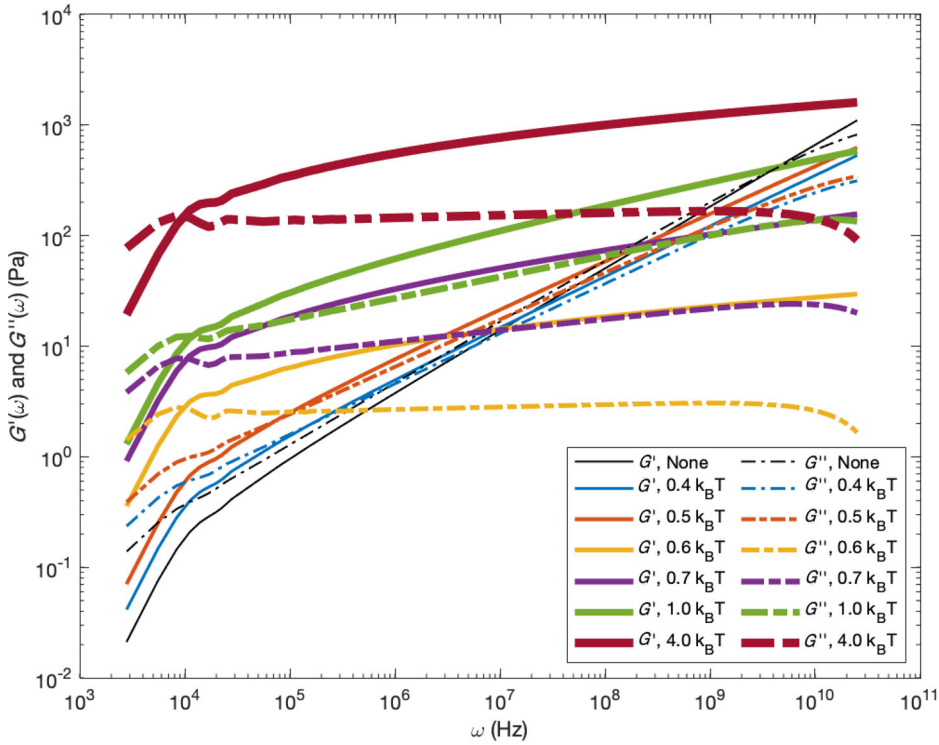

FIGURE 9 The storage modulus (solid lines) and loss modulus (dashed lines) at each interaction strength tested at a concentration of 1.5 mg mucin per ml mucus. Thicker lines correspond to stronger attractive interactions

to beads which appear on separate chains (Figure 7b), showing that separate chains are linking together to form the mucin structures which appear in the visualizations of the model.

To determine if the structures emerging from our simulations indeed resemble those in native airway mucus, we imaged mucus from HBE cells via SEM. Images show a mucus network and condensed native flakes (Figure 4) that are visually similar to specific simulated results in Figure 6, and suggesting at 5.0 mg/ml concentration an estimate of interaction strengths in the potentials governing electrostatic and hydrophobic domain interactions. At 1.5 mg/ml, a dense flake-like structure requires unrealistic 4.0 k_BT interactions with only a hint of a structure transition starting to emerge with 0.7 k_BT interactions (Figure 5). At 5.0 mg/ml, for interactions of 0.4 k_BT (Figure 6a,b), no visible structures form; for interaction strengths of 0.5 k_BT and above (Figure 6c–f), various condensed structures self-organize.

The rheological data computed for the two models further reinforces the structure properties and structure transitions inferred from video analysis of the position data from the models. In the 1.5 mg/ml simulations (9): for the baseline (zero interaction strength), the lower frequencies are sol-like until frequency $\sim 10^7$ Hz and then weakly gel-like at higher frequencies; then for 0.4 and 0.5 k_BT interactions, a similar behavior emerges except the sol–gel transition shifts to lower frequencies. In all three cases, G' and G'' are relatively close to one another, with $\tan\delta$ close to 1 except at the lowest frequencies where the simulation data are less resolved. Then at 0.6 k_BT and higher interaction strengths, there is a strong transition to a gel-dominated behavior, with a stronger dominance of G' over G'' over a large frequency range above 10^4 where we have the greatest numerical resolution. In the simulations where visible structures appear, gel-like behavior

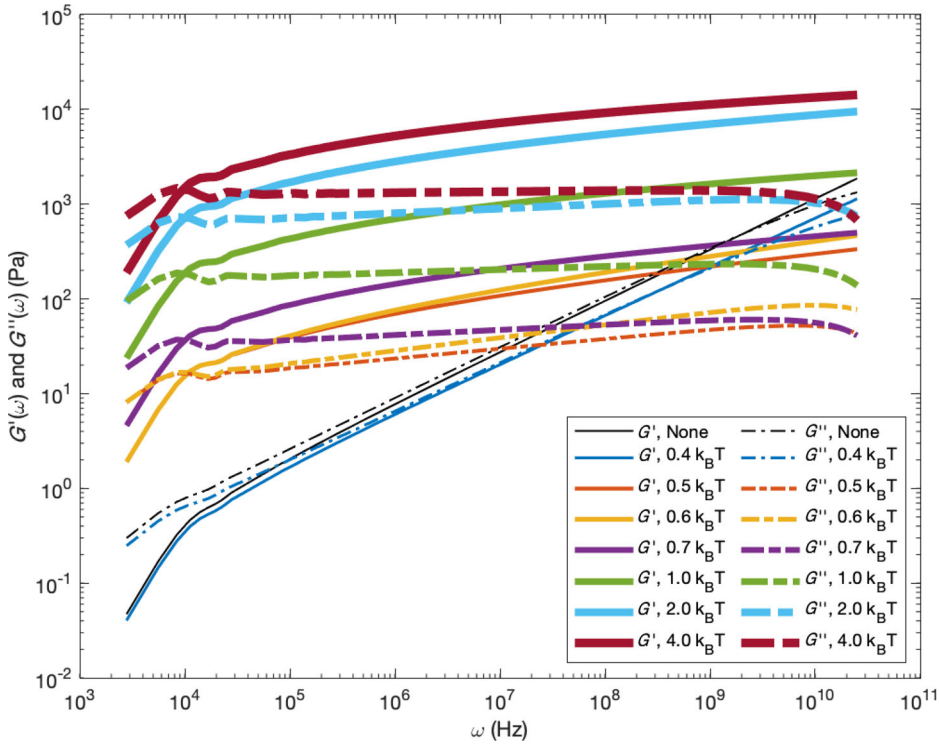

FIGURE 10 The storage modulus (solid lines) and loss modulus (dashed lines) at each interaction strength tested at a concentration of 5.0 mg mucin per ml mucus. Thicker lines correspond to stronger attractive interactions

dominates at the edge of the range of frequencies covered by the simulations, so further coarse-graining will be necessary to evaluate the reliability of this result.

With 5.0 mg/ml mucin concentration, Figure 10 reveals a similar transition versus interaction strength, yet somewhat different in the details. For the baseline zero interaction strength and 0.4 k_BT interaction strength, a weakly sol-like behavior persists over all but the extreme frequencies, with G'' slightly above G' over the $[10^4, 10^9]$ frequency range. Unlike the 1.5 mg/ml data, G'' and G' both *drop slightly* from 0 to 0.4 k_BT interaction strength, and then there is a far more dramatic and monotone shift with a sol–gel transition at 0.6 k_BT and higher. The jump in both G' and G'' from 0.4 to 0.5 k_BT is much higher, with G' dominating G'' at all higher interaction strengths for all frequencies above 10^4 Hz. Once again, the lack of significant numerical resolution and data at long timescales will require further coarse-grained simulations to improve the results below frequencies of 10^4.

When viewing the structures formed by the mucin polymers (Figures 5 and 6) and the dynamic moduli (Figures 9 and 10), it becomes apparent that the presence of visible, permanent flake and network structures in the mucins is reflected through the scaling of G' and G'', both in their raw values and in the power laws they follow. This suggests that, even in the absence of imaging, the rheology of mucus can reflect whether a network of mucus which forms a flake or other structure larger than our simulation domain is present within it.

Notably, the simulations with 0.5 k_BT electrostatic and 0.5 k_BT hydrophobic interactions exhibit an obvious change in both structure and rheology as the mucin concentration increases from 1.5 to 5.0 mg/ml. In the 1.5 mg/ml simulation at this concentration (Figure 5c), no visible structures

are formed, and the dynamic moduli G' and G'' (Figure 9) resemble those of the simulation at 1.5 mg/ml with slightly weaker (0.4 k_BT) interactions. In contrast, the simulation with 0.5 k_BT electrostatic and hydrophobic interactions at a mucin concentration of 5.0 mg/ml exhibits a flake-like structure (Figure 6c) when imaged, and its rheology (Figure 10) resembles that of the simulation with stronger (0.6 k_BT) interactions, not that of the simulation with weaker (0.4 k_BT) interactions. This transition, with interaction strengths kept constant on a pairwise basis, suggests that concentration itself may drive transitions in structure and rheology, independent of other chemical and physical changes in mucus.

It should be noted that the frequencies currently measured by the model exist outside of the range of timescales that can currently be detected by rheometers. Further coarse-graining, done carefully and faithfully to the chemistry of mucin polymers, is necessary to bridge the gap between frequencies that can be measured experimentally and the frequencies resolved by MD simulations.

The dependence on mucin concentrations is consistent with data on mucus samples found from other sources; in purified gastric mucin, aggregation of mucins into larger structures occurs at a mucin weight percentage of 0.5–1.0%,[37] closely approximating the results suggested by this model of HBE mucus.

4 | CONCLUSIONS

The concentration of mucins and the strength of chemical interactions both play a role in determining the morphology and rheology of structures found within HBE mucus. Our results demonstrate that mucus concentration plays a significant role in determining the morphology and rheology of these structures for at least one set of interaction strengths tested in our model, suggesting that mucin concentration alone is enough to affect structure transitions within HBE mucus under certain conditions. We assert this with the caveat that the set of interaction strengths under which this transition occurs are not definitely proven to be the true interaction strengths in physical HBE mucus samples. In addition, these results establish a link between the power laws of the dynamic elastic and viscous moduli and the formation of mucins into flake-like or network-like structures within HBE mucus. Here, we have implemented the first (to our knowledge) stochastic bead-spring, Rouse-like statistical physics model faithful to the chemical structure and properties of the predominant gel-forming mucin MUC5B in airway mucus. We show that at certain interaction strengths and for healthy versus pathological mucin concentrations, the structure morphologies match experimental electron microscopy images from HBE mucus. Furthermore, the data from the MD model allow computation of the frequency-dependent elastic and viscous moduli of the simulated airway mucus, revealing a rheological sol–gel transition across a wide frequency range that coincides with the structure transition. The range of frequencies from these MD simulations are necessarily limited to high frequencies due to numerical stability constraints on the short time steps imposed by resolution of the chemical structure of MUC5B mucin polymers. These timescales are far shorter than those accessible by particle tracking microrheology or other methods performed on physical samples, requiring experiments with different techniques to test the accuracy of our rheological predictions. These results and methods will continue to be refined with more chemical details, for example, inclusion of the less prevalent gel-forming mucin, MUC5AC, as well as other molecular species such as DNA fragments. Our hope is that these findings will guide mucolytic drug strategies to reverse the progression of pathological mucus (the so-called flake burden) in CF. Similar approaches are possible to understand mucus pathology in other lung disorders such as asthma and COPD.

ACKNOWLEDGMENTS

This research was supported in part by grants Cystic Fibrosis Foundation BOUCHE19R0, CFF BOUCHE19XX0, CFF FREEMA19G0, CFF HILL20Y2-OUT, CFF KATO20F0, CFF MARKOV18F0, the National Center for Advancing Translational Sciences (NCATS), National Institutes of Health, through Grant Award Number P01 HL108808, NIH R01 HL136961, NIH UH3 HL123645, NIH UL1 TR002489, NIH NIDDK P30 DK065988, NSF DMS-2028758, NSF CISE-1931516, and NSF DMS-1664645. SEM work was performed at the Chapel Hill Analytical and Nanofabrication Laboratory (CHANL), a member of the North Carolina Research Triangle Nanotechnology Network (RTNN), which is funded by the National Science Foundation (NSF) (Grant ECCS-1542015) as part of the National Nanotechnology Coordinated Infrastructure (NNCI). Computational resources and support were provided by the University of North Carolina at Chapel Hill and its Research Computing group through the Dogwood computing cluster. This paper is our contribution to the special issue in honor of Harvey Segur on the occasion of his 80th birthday. Harvey has been an inspiration, professionally and otherwise, to the last author, Greg Forest, beginning with reading Harvey's work on solitons and nonlinear waves while a graduate student, and amplified through decades of friendship.

DATA AVAILABILITY STATEMENT

The data that support the findings of this study and scripts used to generate and analyze the data are available from the corresponding author upon reasonable request.

REFERENCES

1. Dekker J, Rossen JWA, Büller HA, Einerhand AWC. The MUC family: an obituary. *Trends Biochem Sci*. 2002; 27.3:126–131.
2. van de Bovenkamp JHB, Hau CM, Strous GJAM, Büller HA, Dekker J, Einerhand AWC. Molecular cloning of human gastric mucin MUC5AC reveals conserved cysteine-rich D-domains and a putative leucine zipper motif. *Biochem Biophys Res Commun*. 1998; 245.3:853–859.
3. Escande F, Aubert JP, Porchet N, Buisine MP. Human mucin gene MUC5AC: organization of its 5′-region and central repetitive region. *Biochem J*. 2001; 358.3:763–772.
4. Desseyn JL, Guyonnet-Dupérat V, Porchet N, Aubert JP, Laine A. Human mucin gene MUC5B, the 10.7-kb large central exon encodes various alternate subdomains resulting in a super-repeat. *J Biol Chem*. 1997; 272.6:3168–3178.
5. Offner GD, Nunes DP, Keates AC, Afdhal NH, Troxler RF. The amino-terminal sequence of MUC5B contains conserved multifunctional D domains: implications for tissue-specific mucin functions. *Biochem Biophys Res Commun*. 1998; 251.1:350–355.
6. Desseyn JL, Buisine MP, Porchet N, Aubert JP, Laine A. Genomic organization of the human mucin gene MUC5B. *J Biol Chem*. 1998; 273.46:30157–30164.
7. Bansil R, Turner BS. The biology of mucus: composition, synthesis and organization. *Adv Drug Deliv Rev*. 2018; 124:3–15.
8. Kesimer M, Ford AA, Ceppe A, et al.. Airway mucin concentration as a marker of chronic bronchitis. *N Engl J Med*. 2017; 377.10:911–922.
9. Radicioni G, Cao R, Carpenter J, et al.. The innate immune properties of airway mucosal surfaces are regulated by dynamic interactions between mucins and interacting proteins: the mucin interactome. *Mucosal Immunol*. 2016; 9.6:1442–1454.
10. Kirkham S, Sheehan JK, Knight D, Richardson PS, Thornton DJ. Heterogeneity of airways mucus: variations in the amounts and glycoforms of the major oligomeric mucins MUC5AC and MUC5B. *Biochem J*. 2002; 361.3:537–546.
11. Boucher RC. Molecular insights into the physiology of the "thin film" of airway surface liquid. *J Physiol*. 1999; 516.3:631–638.

12. Knowles MR, Boucher RC. Mucus clearance as a primary innate defense mechanism for mammalian airways. *J Clin Investig*. 2002; 109.5:571–577.
13. Boucher RC. An overview of the pathogenesis of cystic fibrosis lung disease. *Adv Drug Deliv Rev*. 2002; 54.11:1359–1371.
14. Henderson AG, Ehre C, Button B, et al.. Cystic fibrosis airway secretions exhibit mucin hyperconcentration and increased osmotic pressure. *J Clin Investig*. 2014; 124.7:3047–3060.
15. Fahy JV, Dickey BF. Airway mucus function and dysfunction. *N Engl J Med*. 2010; 363.23:2233–2247.
16. Esther CR, Muhlebach MS, Ehre C, et al. Mucus accumulation in the lungs precedes structural changes and infection in children with cystic i. *Sci Transl Med*. 2019;11(486):eaav3488. https://stm.sciencemag.org/content/11/486/eaav3488
17. Iravani J, Van As A. Mucus transport in the tracheobronchial tree of normal and bronchitic rats. *J Pathol*. 1972; 106(2):81–93.
18. Hollander F. The two-component mucous barrier. *AMA Arch Intern Med*. 1954; 93(1):107–120.
19. Strous GJ, Dekker J. Mucin-type glycoproteins. *Crit Rev Biochem Mol Biol*. 1992; 27.1-2:57–92.
20. Perez-Vilar J, Hill RL. The structure and assembly of secreted mucins. *J Biol Chem*. 1999; 274(45):31751–31754.
21. Barz B, Turner BS, Bansil R, Urbanc B. Folding of pig gastric mucin non-glycosylated domains: a discrete molecular dynamics study. *J Biol Phys*. 2012; 38(4):681–703. https://doi.org/10.1007/s10867-012-9280-x
22. Bansil R, Turner BS. Mucin structure, aggregation, physiological functions and biomedical applications. *Curr Opin Colloid Interface Sci*. 2006; 11.2-3:164–170.
23. Turner BS. *Expression of Cysteine-Rich Pig Gastric Mucin (Muc5AC) Domains in Pichia pastoris and Their pH-Dependent Properties*. PhD thesis, Boston University; 2012.
24. Bhaskar KR, Gong DH, Bansil R, et al.. Profound increase in viscosity and aggregation of pig gastric mucin at low pH. *Am J Physiol Gastrointest Liver Physiol*. 1991; 261(5):G827–G832.
25. Cao X, Bansil R, Bhaskar KR, et al.. pH-dependent conformational change of gastric mucin leads to sol-gel transition. *Biophys J*. 1999; 76(3):1250–1258.
26. Celli JP, Turner BS, Afdhal NH, et al. Rheology of gastric mucin exhibits a pH-dependent sol-gel transition. *Biomacromolecules*. 2007; 8(5):1580–1586. https://doi.org/10.1021/bm0609691
27. Hong Z, Chasan B, Bansil R, Turner BS, Bhaskar KR, Afdhal NH. Atomic force microscopy reveals aggregation of gastric mucin at low pH. *Biomacromolecules*. 2005; 6(6):3458–3466.
28. Cao X. *Aggregation and Gelation of Mucin and Its Interactions with Lipid Vesicles*. PhD thesis, Boston University; 1997.
29. Berendsen HJC, van der Spoel D, van Drunen R. GROMACS: a message-passing parallel molecular dynamics implementation. *Comput Phys Commun*. 1995; 91.1-3:43–56.
30. Lindahl E, Hess B, van der Spoel D. GROMACS 3.0: a package for molecular simulation and trajectory analysis. *J Mol Model*. 2001; 7(8):306–317.
31. Shah VS, Meyerholz DK, Tang XX, et al. Airway acidification initiates host defense abnormalities in cystic fibrosis mice. *Science*. 2016; 351(6272):503–507. https://doi.org/10.1126/science.aad5589
32. Hill DB, Long RF, Kissner WJ, et al.. Pathological mucus and impaired mucus clearance in cystic fibrosis patients result from increased concentration, not altered pH. *Eur Respir J*. 2018; 52(6):1801297.
33. Hill DB, Vasquez PA, Mellnik J, et al. A biophysical basis for mucus solids concentration as a candidate biomarker for airways disease. *PLoS One*. 2014;9(2):e87681. https://doi.org/10.1371/journal.pone.0087681
34. Levy R, Hill DB, Forest MG, Grotberg JB. Pulmonary fluid flow challenges for experimental and mathematical modeling. *Integr Comp Biol*. 2014; 54(6):985–1000. https://doi.org/10.1093/icb/icu107
35. Vasquez PA, Forest MG. *Complex Fluids and Soft Structures in the Human Body*. Springer Series on Biological and Medical Physics. Springer; 2015.
36. Vasquez PA, Jin Y, Palmer E, Hill D, Forest MG. Modeling and simulation of mucus flow in human bronchial epithelial cell cultures - part 1: idealized axisymmetric swirling flow. *PLoS Comput Biol*. 2016;12(8):e1004872. https://doi.org/10.1371/journal.pcbi.1004872
37. Lafitte G, Sderman O, Thuresson K, Davies J. PFG-NMR diffusometry: a tool for investigating the structure and dynamics of noncommercial purified pig gastric mucin in a wide range of concentrations. *Biopolymers*. 2007; 86(2):165–175. https://onlinelibrary.wiley.com/doi/abs/10.1002/bip.20717
38. Lai SK, Wang YY, Hanes J. Mucus-penetrating nanoparticles for drug and gene delivery to mucosal tissues. *Adv Drug Deliv Rev*. 2009; 61(2):158–171. https://doi.org/10.1016/j.addr.2008.11.002

39. Newby JM, Seim I, Lysy M, et al.. Technological strategies to estimate and control diffusive passage times through the mucus barrier in mucosal drug delivery. *Adv Drug Deliv Rev*. 2018; 124:64–81.
40. Suk JS, Xu Q, Kim N, Hanes J, Ensign LM. PEGylation as a strategy for improving nanoparticle-based drug and gene delivery. *Adv Drug Deliv Rev*. 2016;99:28–51. https://doi.org/10.1016/j.addr.2015.09.012
41. Bird RB, Armstrong RC, Hassager O. *Dynamics of Polymeric Liquids*. Vol. 1. Wiley; 1987.
42. Bird RB, Armstrong RC, Hassager O. *Dynamics of Polymeric Liquids*. Vol. 2. Wiley; 1987.
43. Kremer K, Grest GS. Dynamics of entangled linear polymer melts: a molecular dynamics simulation. *J Chem Phys*. 1990; 92(8):5057–5086.
44. Plimpton S. Fast parallel algorithms for short-range molecular dynamics. *J Comput Phys*. 1995; 117(1):1–19.
45. Symmes BA, Stefanski AL, Magin CM, Evans CM. Role of mucins in lung homeostasis: regulated expression and biosynthesis in health and disease. *Biochem Soc Trans*. 2018; 46(3):707–719.
46. Schulz BL, Sloane AJ, Robinson LJ, et al.. Glycosylation of sputum mucins is altered in cystic fibrosis patients. *Glycobiology*. 2007; 17(7):698–712.
47. Chace KV, Leahy DS, Martin R, Carubelli R, Flux M, Sachdev GP. Respiratory mucous secretions in patients with cystic fibrosis: relationship between levels of highly sulfated mucin component and severity of the disease. *Clin Chim Acta*. 1983; 132(2):143–155.
48. Hughes GW, Ridley C, Collins R, Roseman A, Ford R, Thornton DJ. The MUC5B mucin polymer is dominated by repeating structural motifs and its topology is regulated by calcium and pH. *Sci Rep*. 2019; 9(1):17350:1–13.
49. Georgiades P, Di Cola E, Heenan R, Pudney P, Thornton D, Waigh T. A combined small-angle X-ray and neutron scattering study of the structure of purified soluble gastrointestinal mucins. *Biopolymers*. 2014; 101:1154–1164.
50. Schneider T, Stoll E. Molecular-dynamics study of a three-dimensional one-component model for distortive phase transitions. *Phys Rev B*. 1978; 17(3):1302–1322.
51. Dünweg B, Paul W. Brownian dynamics simulations without Gaussian random numbers. *Int J Mod Phys C*. 1991; 2(3):817–827.
52. Witten J, Samad T, Ribbeck K. Molecular characterization of mucus binding. *Biomacromolecules*. 2019; 20(4):1505–1513.
53. Sandia Corporation. LAMMPS documentation. https://lammps.sandia.gov/doc/units.html
54. Humphrey W, Dalke A, Schulten K. VMD: visual molecular dynamics. *J Mol Graph*. 1996; 14(1):33–38. http://www.sciencedirect.com/science/article/pii/0263785596000185
55. Cao X, Forest MG. Rheological tuning of entangled polymer networks by transient cross-links. *J Phys Chem B*. 2019; 123(5):974–982.
56. Rubinstein M, Colby RH. *Polymer Physics*. Oxford University Press; 2003.
57. Thompson AP, Plimpton SJ, Mattson W. General formulation of pressure and stress tensor for arbitrary many-body interaction potentials under periodic boundary conditions. *J Chem Phys*. 2009; 131(15):154107.
58. Likhtman AE, Sukumaran SK, Ramirez J. Linear viscoelasticity from molecular dynamics simulation of entangled polymers. *Macromolecules*. 2007; 40(18):6748–657.

SUPPORTING INFORMATION

Additional supporting information may be found online in the Supporting Information section at the end of the article.

How to cite this article: Ford AG, Cao X-Z, Papanikolas MJ, Kato T, Boucher RC, Markovetz MR, Hill DB, Freeman R, Forest MG. Molecular dynamics simulations to explore the structure and rheological properties of normal and hyperconcentrated airway mucus. *Stud Appl Math*. 2021;1–19. https://doi.org/10.1111/sapm.12433